JOURNAL OF GEOPHYSICAL RESEARCH, VOL. 112, D24S20, doi:10.1029/2007JD008742, 2007

Remote sensing of Greenland ice sheet using multispectral near-infrared and visible radiances

Petr Chylek,[1] M. McCabe,[1,2] M. K. Dubey,[2] and J. Dozier[3]

Received 2 April 2007; revised 21 June 2007; accepted 19 November 2007; published 14 December 2007.

[1] We present the physical basis of and validate a new remote-sensing algorithm that utilizes reflected visible and near-infrared radiation to discriminate between dry and wet snow. When applied to the Moderate Resolution Imaging Spectroradiometer (MODIS) satellite data, our discrimination algorithm has the potential to retrieve melting regions of the ice sheet at a spatial resolution of 0.25 km^2, over three orders of magnitude higher than the resolution of current microwave methods. The method should be useful for long-term monitoring of the melt area of the Greenland ice sheet, especially regions close to ice sheet margins and of the outflow glaciers. Our analysis of MODIS retrievals of the western portion of the Greenland ice sheet over the period 2000 to 2006 indicates significant interannual variability with a maximum melt extent in 2005. Collocated in situ meteorological data reveal a high correlation (0.80) between the MODIS melt-day area and the average summer temperature. Our analysis suggests that it is the magnitude of the summer temperature that dominates the melting (not the variability of the length of the melting season). Furthermore, we find that the melt-day area increases by about 3.8% for each 0.1 K increase in the average surface air summer temperature. We combine this empirical relationship with historic temperature data to infer that the melt-day area of the western part of the ice sheet doubled between the mid-1990s and mid-2000s and that the largest ice sheet surface melting probably occurred between 1920s and 1930s, concurrent with the warming in that period.

Citation: Chylek, P., M. McCabe, M. K. Dubey, and J. Dozier (2007), Remote sensing of Greenland ice sheet using multispectral near-infrared and visible radiances, *J. Geophys. Res.*, *112*, D24S20, doi:10.1029/2007JD008742.

1. Introduction

[2] The present atmospheric concentration of carbon dioxide is about 380 ppmv (parts per million by volume) compared to about 280 ppmv during the pre-industrial era. Currently, about a half of the anthropogenic CO_2 produced by fossil fuel combustion stays in the atmosphere, leading to an annual increase of around 2 ppmv per year. With rapidly increasing economic growth of developing countries it is expected that atmospheric CO_2 concentrations will continue to increase over the coming decades. It is anticipated that atmospheric CO_2 concentration will double and perhaps triple their pre-industrial levels before the end of this century.

[3] Global climate models predict a gradual increase in global mean surface temperature, with a much more rapid temperature rise in polar regions. In the areas of Greenland that are not affected by North Atlantic Oscillations (NAO), the rate of temperature increase was confirmed to be more than double that of global temperature increases [*Chylek and Lohmann*, 2005]. Greenland temperature has risen dramatically during the past decade, although during the 1920–1940s Greenland temperatures were even higher than are currently being observed [*Vinther et al.*, 2006; *Chylek et al.*, 2006a]. The Greenland mass balance has recently shifted from positive (increasing) [*Zwally et al.*, 2005; *Johannessen et al.*, 2005] to negative (decreasing) values [*Hanna et al.*, 2005; *Luthcke et al.*, 2006], raising the possibility of sustained warming and melting of the Greenland ice sheet. Unfortunately, understanding and predicting the response of polar region to CO_2 radiative forcing is limited by an incomplete understanding of the dynamic nature of ice sheet behavior. The melting of the ice sheets is one of the most drastic possible outcomes of global warming. Ice sheet melting would raise sea levels, the influx of fresh-water could slow the oceanic thermohaline circulation, and land-cover changes could trigger positive albedo feedbacks when reflective ice surfaces are replaced by darker vegetation. Consequently, there is a need to accurately monitor the state of the Greenland ice sheet as a whole, and in particular, smaller areas close to ice sheet margins and in outflow glaciers where accelerated melting and outflow has been recently observed.

[4] Current methods for monitoring the ice sheet melt area generally employ microwave wavelengths [*Abdalati*

[1]Space and Remote Sensing, Los Alamos National Laboratory, Los Alamos, New Mexico, USA.
[2]Earth and Environmental Sciences, Los Alamos National Laboratory, Los Alamos, New Mexico, USA.
[3]Donald Bren School of Environmental Science and Management, University of California, Santa Barbara, Santa Barbara, California, USA.

0148-0227/07/2007JD008742$09.00

and Steffen, 1995, 2001; *Steffen et al.*, 2004; *Ashcroft and Long*, 2006] with a spatial resolution of 625 km^2 (a pixel size of 25 km × 25 km). Considering that the width of the portion of the Greenland ice sheet that is subject to melt is often of the order of 25 to 100 km, and that the outflow regions are only a few km wide, a remote-sensing approach with a higher spatial resolution would advance our knowledge of melt-dynamics in this region. In the range of visible and infrared remote sensing, the Landsat Thematic Mapper has been used to distinguish between snow and cloud cover [*Dozier*, 1989] and the MODIS albedo products were compared with Greenland in situ measurements [*Stroeve et al.*, 2005]. Satellite derived surface temperature [*Stroeve and Steffen*, 1998; *Hall et al.*, 2006] usually have an error in the order of ±2 K in the case of dry snow and a larger error on the boundary between dry and melting snow due to different emissivities, and are thus not an ideal tool to distinguish between snow type.

[5] In this paper we develop an algorithm that is applicable to multispectral (or hyperspectral) satellite instruments, which utilizes the distinct spectral features in reflected visible and near-infrared radiances to discriminate between the ice and water phases at the land surface. When applied to MODIS data, a spatial resolution of either 1 km^2 or 0.25 km^2 is achievable, depending on the level of product utilized. We first validate the algorithm using the high-resolution (5 m in visible and 20 m in infrared) images from the archives of the DOE Multispectral Thermal Imager (MTI) research satellite [*Szymanski and Weber*, 2005]. We then apply our algorithm to available MODIS data to assess the variability of the melt area over the western part of the Greenland ice sheet between the years 2000–2006.

2. Physical Basis of Multispectral Wet/Dry Snow Detection

[6] An algorithm developed recently to distinguish between water, ice and mixed phase clouds [*Chylek and Borel*, 2004; *King et al.*, 2004; *Chylek et al.*, 2006b] or to differentiate fine and wet coarse-grain snow [*Dozier*, 1989; *Dozier and Painter*, 2004] using the near-infrared multispectral bands provides a starting point for our work. Typical values of measured snow and water reflectivity between 1.5 and 2.5 μm region are shown in Figure 1a together with the spectral intervals covered by the MODIS bands 6 and 7 [*King et al.*, 1992; *Tanré et al.*, 1997; *Remer et al.*, 2005].

[7] In the case of melting snow, a "deep" layer of liquid water that is characterized by the reflectivity shown in Figure 1 is not actually present. Water in snow does not necessarily coat the grains unless the water content is quite high. At lower water content the water causes the grains to cluster, optically mimicking a larger grain size [*Colbeck*, 1979; *Dozier and Painter*, 2004]. At higher water content we might have only a thin water layer that covers the snow grains. Satellite instruments can detect this water layer only if the thickness of the layer is of the order of the skin depth. The skin depth, d, at the considered wavelength, λ, is the thickness of a layer within which the electromagnetic wave is attenuated by a factor of e (e being the base of the natural logarithm). The skin depth is given by [*Jackson*, 1975]

$$d = 2\pi\lambda/m_i \tag{1}$$

where m_i is the imaginary part of refractive index of considered material. Using the imaginary part of refractive index of water in the near-infrared region [*Kou et al.*, 1993] we obtain the skin depth of water as shown in Figure 1b. Assuming that the required thickness to be at least $d/10$, the MODIS band 6 can detect a water layer with a thickness $t >$ 160 μm, while the band 7 can detect water layer with a thickness $t > 40$ μm. Consequently, we select MODIS band 7 as a more suitable band to distinguish between dry or wet snow.

[8] To minimize the effects of differences in illumination and scattering by atmospheric aerosols, we use a ratio of reflectances at two wavelengths. We define the Melt Area Detection Index (MADI) as

$$MADI = \frac{R_{0.67}}{R_{2.1}} \tag{2}$$

where $R_{0.67}$ is the reflectance in the MODIS band 1 (620–670 nm) and $R_{2.1}$ is the reflectance in the band 7 (2105–2155 nm). When working with the MTI images [*Szymanski and Weber*, 2005], the MTI band C is used as a reference band and band O to discriminate between water and snow surfaces.

[9] A more subtle effect of melting snow is a slight spectral shift in the absorption coefficient of ice versus liquid water, and there is a similar shift between liquid water and water vapor. Therefore with a hyperspectral sensor one can simultaneously estimate all three phases of water–water vapor in the atmosphere, liquid water in the snow near the surface, and the size of the snow grains [*Green et al.*, 2006]. With a multispectral sensor such as MODIS, one can detect grain coarsening that snowmelt causes as well as, at higher water content, a thin layer (of the order of 10 μm) of liquid water on the snow grains. That is, MODIS detects snow that has been melting.

3. Supporting Observations

[10] To demonstrate the validity of the MADI discrimination method we use high-resolution imagery obtained from the DOE Multispectral Thermal Imager (MTI) research satellite. The advantage of the MTI over MODIS is its high spatial resolution: 5 m in visible and 20 m in the infrared bands. The high resolution retrievable from MTI offers a considerably improved observation/validation capacity relative to MODIS. Through utilizing MTI it is possible to visually distinguish between snow patches and bare land at a resolution of 25 m^2.

[11] Two images in the northeast United States, during different periods of the winter and spring seasons, were chosen for initial analysis. The images were obtained on 14 January 2003 and on 4 April 2002. Both retrievals display patches of surface snow that are clearly visible at the high MTI spatial resolution of 5 m. A 2000 m transect across a patch of snow selected from the 14 January scene is shown in Figure 2g (5 m pixel size spatial resolution). Figures 2a, 2b, and 2c show the reflectivity in the MTI bands C (analogues to the MODIS band 1) and O (analogues to the MODIS band 7), the derived MADI index, together with the 10.5 μm brightness temperature. Values here are shown using the 20 m pixel size resolution.

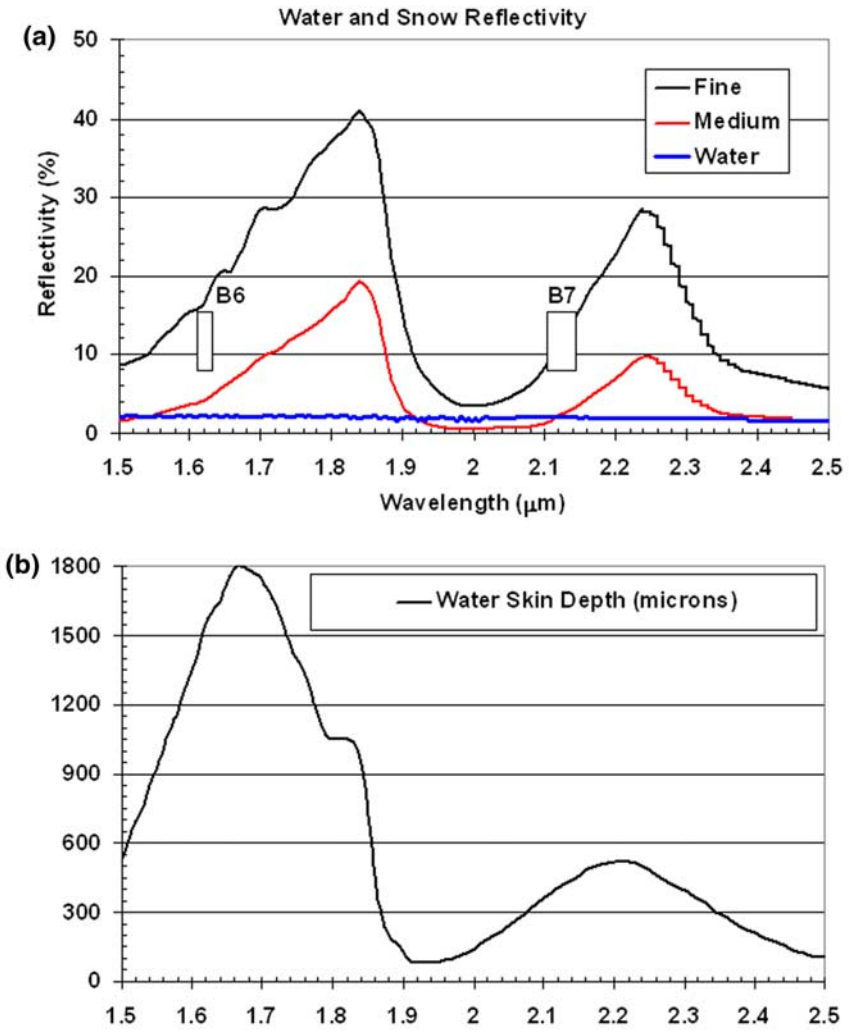

Figure 1. Figure 1a shows the reflectance of water (the thick, almost horizontal line near 2% reflectance value; a blue line in online version) and snow of a fine (thick black line) and medium (thin line; red in online version) size of grains within 1.5 to 2.5 μm spectral range. The data are from the ASTER spectral library. (Reproduced from the ASTER Spectral Library through the courtesy of the Jet Propulsion Laboratory, California Institute of Technology, Pasadena, California. Copyright 1999, California Institute of Technology, all rights reserved). Figure 1b shows the water skin depth as a function of the wavelength.

[12] Due to the high emissivity of both water and snow at 10.5 μm, the brightness temperature at this wavelength is close (within 2 K) to the physical temperature of the water or snow surface. The brightness temperature of the snow patch on 14 January 2003 is between 259–260 K, indicating a cold regime and implying dry rather than melting snow. The brightness temperature of the surrounding bare land is between 260–261 K, also supporting a sub-freezing regime. We note that on this cold and dry day, the values of the MADI over the patch of transect lie between 9–10.

[13] Another patch of snow (much smaller in spatial dimension) was selected from the image obtained on 4 April 2002 (not shown). Figures 2d, 2e, and 2f show reflectivity, MADI and brightness temperature, respectively, for a selected patch of snow on this warm spring day. The reflectivity within the MTI band O is low over the snow patch (Figure 2d) as is expected from the low reflectivity of water in this spectral region. Consequently the values of the MADI index are high (Figure 2e), between 40 and 50, indicating wet snow. This is confirmed by the 10.5 μm brightness temperature that is around 277 K for bare land but drops to about 273.5 K over the snow patch, close to the melting point of ice.

Figure 2. The MTI image of dry snow patches on 14 January 2003 (Figure 2g) used for algorithm validation. The transect T-T shows the path across the snow patch used to acquire the data shown in Figures 2a–2c: the reflectance in the MTI bands C and O along the transect (Figure 2a), the MADI index (Figure 2b), and the 10.5 μm brightness temperature (Figure 2c). Figures 2d–2f show similar data for the wet snow patch (not shown) observed at the same location on 4 April 2002.

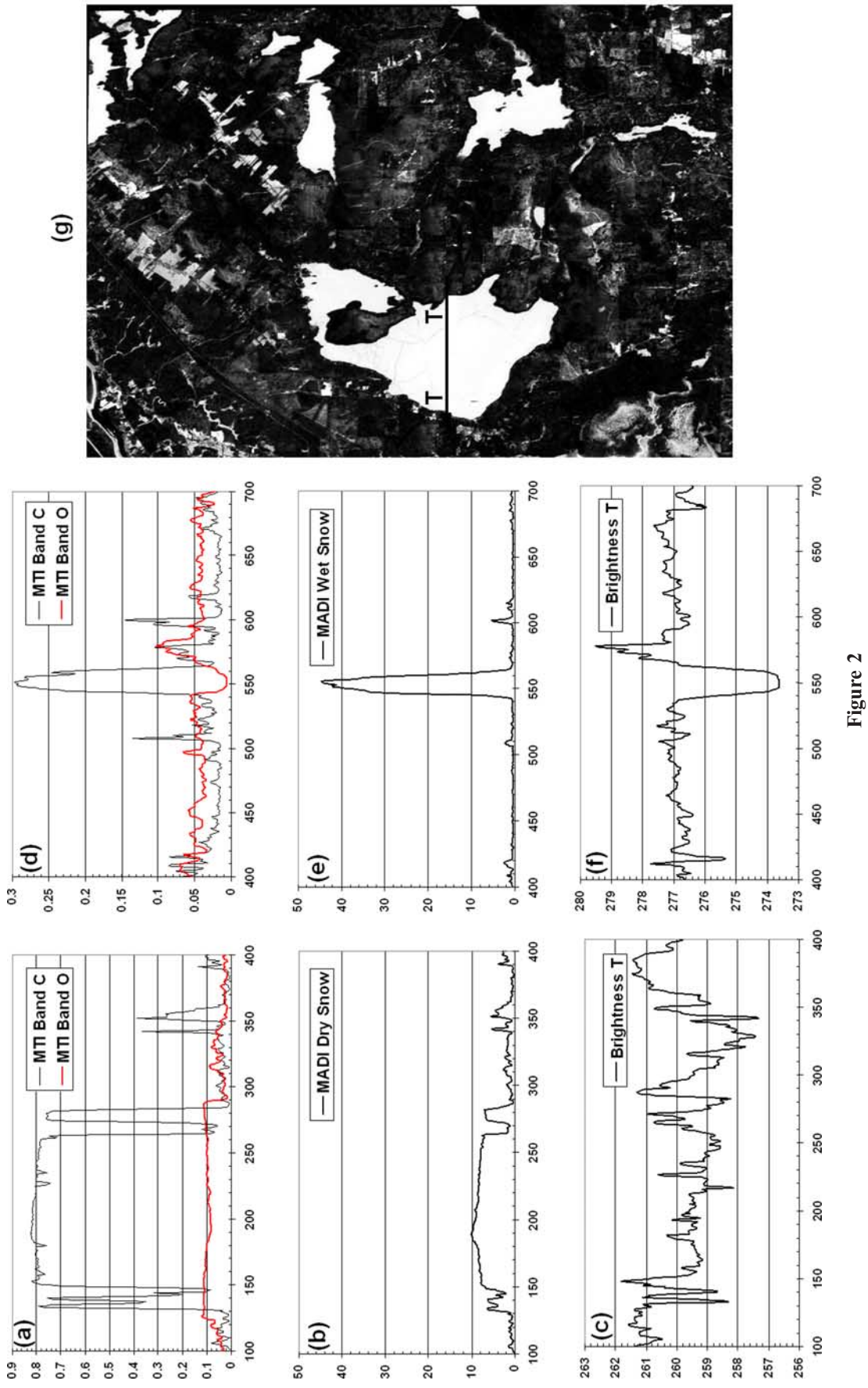
(g)
T
T
(d)
MΠ Band C
MΠ Band O
(e)
MADI Wet Snow
(f)
Brightness T
(a)
MΠ Band C
MΠ Band O
(b)
MADI Dry Snow
(c)
Brightness T

Figure 2

[14] An additional validation of the low values of the MADI for the case of dry snow is provided by the MTI imagery of the summit of the Greenland ice sheet. We have selected a clear sky day image for 12 May 2003 (day 132). Figure 3a shows an image (5 m spatial resolution) of the GISP2 (Greenland Ice Sheet Project 2) ice core drilling site, with a landing strip shown as a straight nonhorizontal line in the top part of the image. The transect denoted by T-T was selected for our dry/wet snow discrimination analysis. The snow and air temperature for the days 11 and 12 May 2003 (days 131 and 132) at the summit were obtained from the AWS (Automated Weather Stations) network on the ice sheet (http://cires.colorado.edu/science/groups/steffen/gcnet/). The values of the MADI index along the T-T direction are plotted in Figure 3c. The low MADI values of between 7–8, indicate dry snow. The AWS temperature records at the summit confirm dry nonmelting conditions, with the temperature in the −25 to −45°C range.

[15] We conclude that the MADI index discriminates between dry and wet snow, showing high values of the index for wet melting snow (as expected from the low reflectivity of water in the near infrared) and considerably lower values for dry snow.

4. Greenland Ice Sheet Melt Detection

[16] An example of the Greenland ice sheet melt area detection is shown in Figure 4. Figure 4a shows the MODIS image of the southern part of Greenland on 17 June 2003. The transect selected for the MADI analysis is shown as a horizontal line denoted as T-T. Figure 4b shows the MADI index along the selected transect. The profile of the MADI index (equation (2)), exhibits a drop close to pixel number 580, indicating a transition from the wet melting snow (high values of the MADI index for pixel numbers <580) to an area of dry snow (with a much lower values of the MADI index for pixel numbers >580). The extremely low values of the MADI index at the left side of Figure 4b correspond to bare land; the edge of an ice sheet is reached close to pixel number 510 at which point the index rises to a high values corresponding to wet melting snow. We emphasize that the sharp drop of the MADI index at the boundary of the wet to dry snow is not detectable using the visible spectral bands alone. It occurs only in the near-infrared bands due to the different reflectivity of water and snow.

[17] A comparison of the MADI dry/wet snow detection over the western part of the Greenland ice sheet with the microwave AMSR-E (Advanced Microwave Scanning Radiometer-E) method (Figure 5) shows that both methods detect melting in the same area, however the MADI provides much finer details and higher total melt area accuracy.

5. Coastal Greenland Temperatures and the Melt-Day Area

[18] MODIS data, available since 24 February 2000, provide an opportunity to examine the interannual variability of the melt area with high spatial resolution. The melt-day area (melt-day area is determined by calculating the number of days that each pixel is characterized to be melting and multiplying that by the 1 km^2 pixel area, and then summing across all pixels) for the years 2000–2006 is shown in Figure 6. Figure 6 displays cumulative melt area calculated from data collected over the western part of the Greenland ice sheet (between 67N and 76N) from MODIS-Terra imagery during the months May–September, over the years 2000–2006. The color code relates the number of melting days detected for individual 1 km^2 pixels, with blue corresponding to a large number of days and red to just a day or two over the entire summer melting season. Within the years 2000–2006 the 2005 was the year of maximum melt in this western part of the ice sheet (Figure 7). However, the melt-day area decreased significantly (by over 25%) in 2006.

[19] The MADI/MODIS spatial resolution of 1 km^2 enhances the accuracy of the detected melt area and allows a meaningful investigation of the regional melt area versus temperature relationship. Within the latitudinal belt there is a coastal meteorological station at Egedesminde (68°42′N, 52°45′W) that provides a continuous temperature record since 1950. We use the annual average summer temperature (June, July, and August (JJA)) to characterize the interannual seasonal temperature and melt area variability. We find the melt-day area to be correlated with the summer temperature at the adjacent coastal station (Figure 7). The correlation coefficient of 0.80 suggests that warm air advected from over the ocean initiates the melting of the ice sheet.

[20] The AMSR-E microwave data are available from the year 2002. Although both MADI and AMSR-E data show a maximum melt in the year 2005 (which is also a year of the highest temperature at Egedesminde), there are substantial differences between the data obtained with the AMSR-E resolution of 625 km^2 and with MADI resolution of 1 km^2. The correlation coefficient between MADI melt-day area and the coastal station summer (JJA) temperature (Egedesminde) for the years 2002–2006 increases to 0.91, while the correlation between the summer temperature and the AMSR determined melt-day area is only 0.47. This result suggests that the high-resolution MADI determination of the melt area captures important details, which are missed by the coarser AMSR-E, which makes the results more correlated with the temperature record (Table 1).

[21] Furthermore, the slope of the line fit to the relative melt-day area and average summer temperature (Figure 7c), identifies an important empirical physical property of the western part of the ice sheet, namely for a temperature increase/decrease of 0.1 K the melt-day area increases/decreases by about 3.8%.

6. Past Melt Area Estimates

[22] We use the derived empirical relation between the coastal air temperature and melt-day area to estimate the past melting extent of the Greenland ice sheet. The average JJA temperature at Egedesminde (68°42′N, 52°45′W) and Godthaab Nuuk (64°10′N, 51°45′W) is shown in Figure 8a. Figure 8b shows a reconstructed melt-day area using the temperature records and 3.8%/0.1 K relationship. A dramatic temperature increase observed over Greenland in the last decade, suggests more than doubling of the melt-day area (and water runoff) since early 1990s. This rapid increase in melting observed during the last decade might not be unprecedented in Greenland history. Temperature

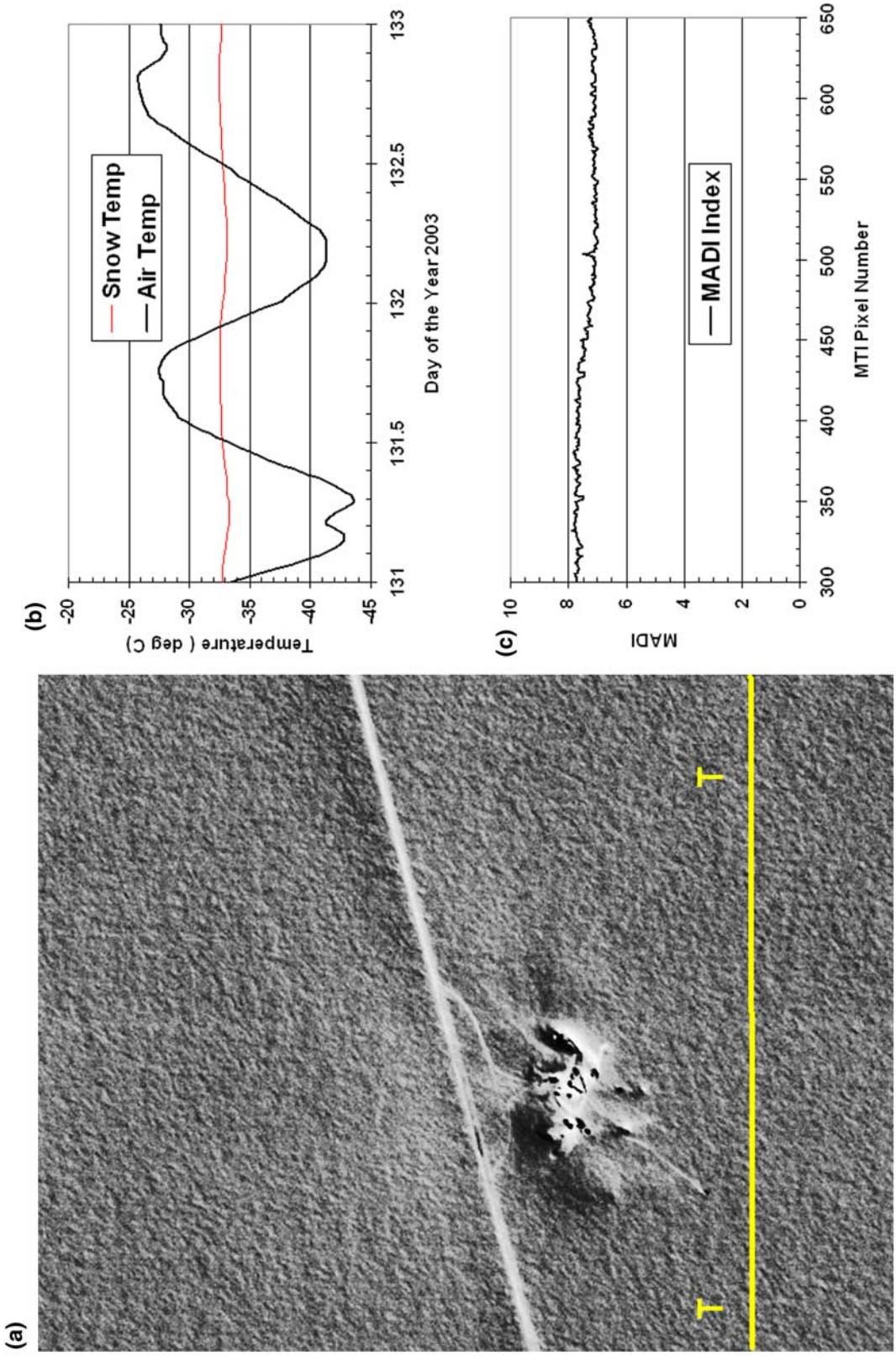

Figure 3. The DOE Multispectral Thermal Imager (MTI) satellite image of the summit of the Greenland ice sheet (5 m spatial resolution) and the transect T-T used for the Melt Area Detection Index (MADI) analysis (Figure 3a). The temperature recorded (Figure 3b) on the same day (day 132) by the Automated Weather System (AWS) station at the summit suggests deep freezing without any chance of melting. The low values of the MADI index (Figure 3c) suggest dry, nonmelting snow.

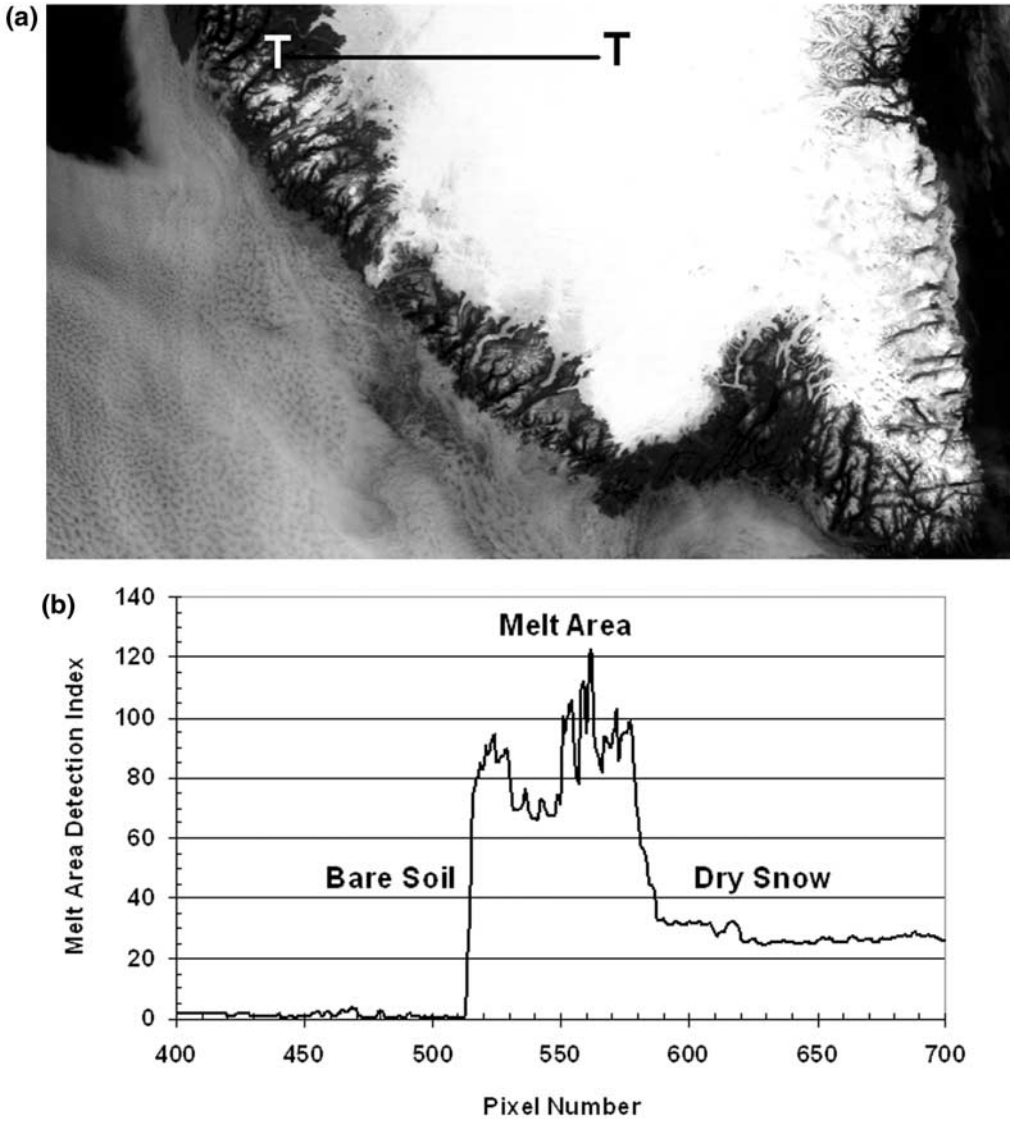

Figure 4. The MODIS image of the southern part of Greenland on 17 June 2003 (Figure 4a) and the transect T-T used for the MADI analysis. The value of the MADI index (Figure 4b) indicates the bare land for pixel numbers <510, melting ice sheet for pixel numbers approximately between 510 and 585, and dry ice sheet for pixel numbers >585.

records suggest [*Vinther et al.*, 2006; *Chylek et al.*, 2006a] that the Greenland temperature during 1930s and 1940s was higher than today and that the rates of warming were similar to those observed during the past decade. Our empirically derived relation between temperature increase and increase in melt area suggests that the western part of the Greenland ice sheet at that time might have experienced surface melting rates that were even higher than present rate (Figure 8). Although we have no objective measurements of melting and ice mass balance during that time, a 1948 article [*Ahlmann*, 1948, p. 183] reports, "The last decades have reduced the ice in some parts of Greenland to such an extent that the whole landscape has changed in character. " This eyewitness account [*Ahlmann*, 1948] suggests that an accelerated ice melting in Greenland in the 1920s and 1930s indeed occurred, as suggested by our temperature/melt area relation. An important historical fact is that this decades long Greenland warming apparently did not exceed a threshold for rapid ice sheet disintegration as evidenced by the ice sheet stabilization and re-growth that followed. This qualitative finding is important to be quantified in the future and be included in models to better predict the vulnerability of the ice sheet to anthropogenic climate change.

7. Length of Melting Season

[23] The ice sheet melt area is affected by the temperature during the melt season and by the length of melting season. A key question is which of the two factors dominates? Figure 9 shows the average April–May and September–October temperature at Godthaab Nuuk station. We note that the recent average of the September–October temperature reaches the value it had in 1930s, while the recent

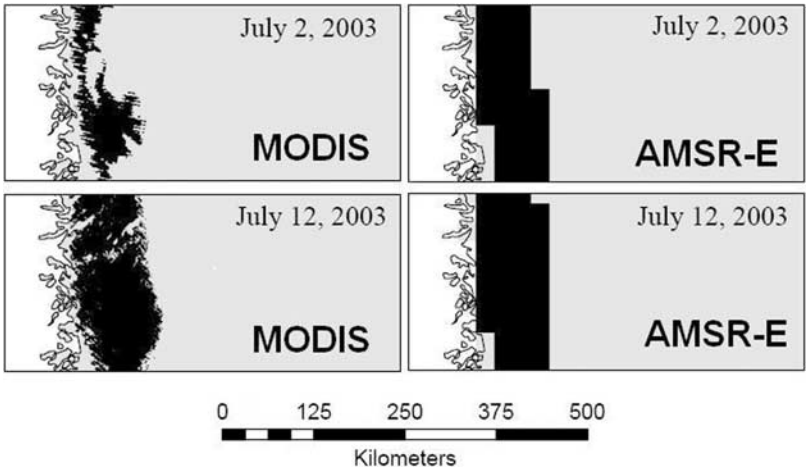

Figure 5. A comparison of MODIS/MADI and AMSR-E derived melt area for 2 and 12 July 2003 over a portion of the northwest coast of Greenland, situated approximately between latitudes 72.5 and 74.5N.

April–May temperature, in spite of its fast increase between 1991 and 1996, is still about 1.5°C below its 1930s values. Judging from the absolute values of the fall and spring temperatures (Figure 9) it seems that the fall season has a better chance to prolong the melting season then the spring, at least at the western part of Greenland.

[24] We have seen that the summer temperature (JJA) at Egedesminde correlates well with the melt-day area, with correlation coefficient 0.80 for the years 2000–2006. On the other hand neither the spring, nor the fall temperature shows any correlation with the melt-day area of the western part of the Greenland ice sheet. The correlation coefficient between melt-day area and the temperature averaged over the four considered months (April, May, September and October) is 0.002. Consequently we conclude that it is the absolute value of the summer temperature that dominates the variability of the western part of the ice sheet. The length of the melt season plays a secondary role.

8. Conclusion

[25] The MODIS radiances in visible and near-infrared bands provide a valuable tool for high spatial resolution (1 km^2 or 0.25 km^2) monitoring of the Greenland ice sheet

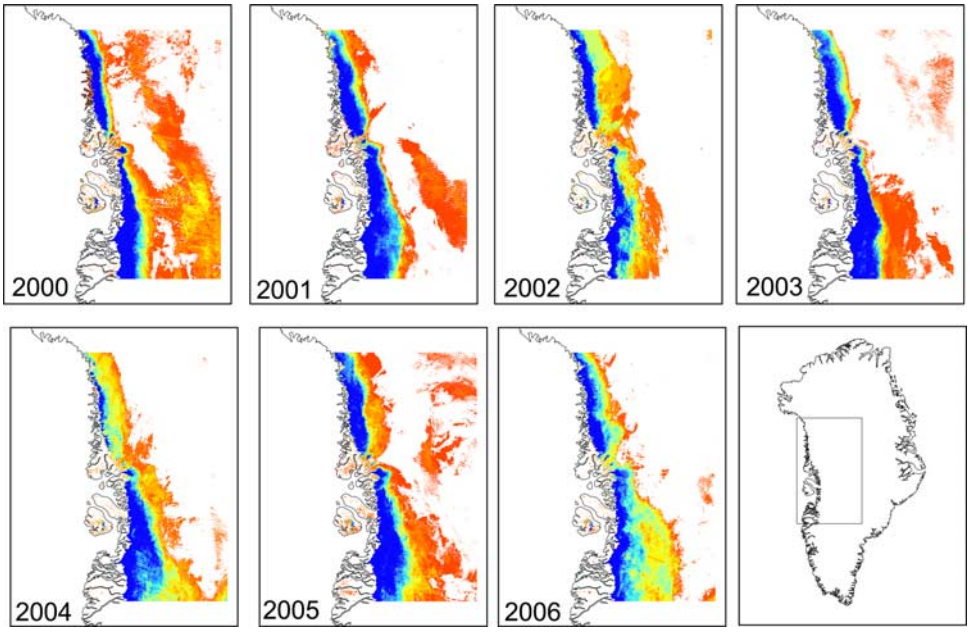

Figure 6. The melt-day area as detected using the MADI method and the MODIS radiances over the western part of the Greenland ice sheet between latitudes 67.0 and 76.0N for the years 2000–2006. The shading indicates number of melt days with black (blue in color version) indicating melting during more then 20 days, dark gray 11 to 20, and light gray (red in color version) 1 to 10 detected melt days of individual 1 km^2 pixels.

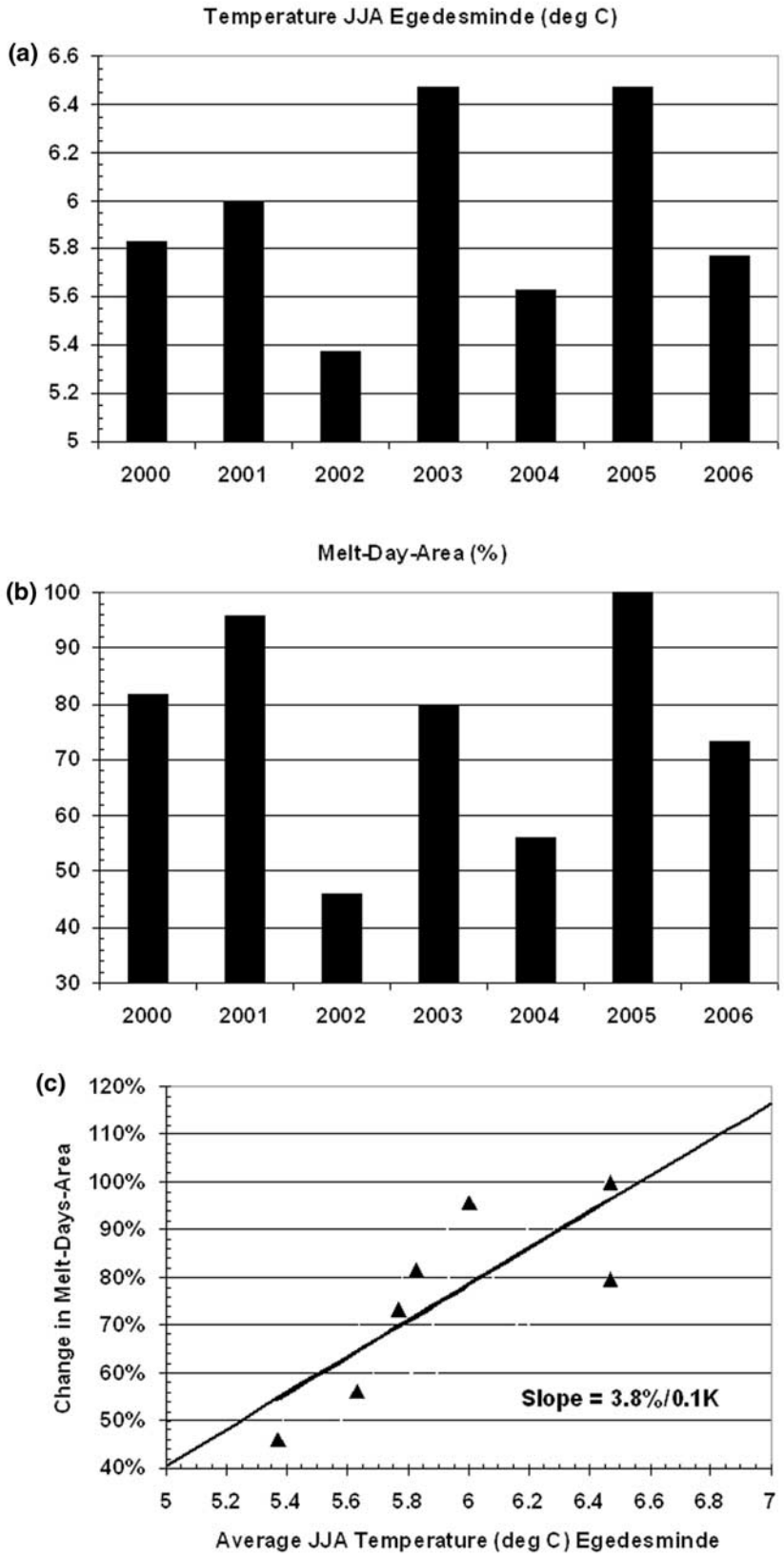

Figure 7. The average summer (June, July, and August) air temperature at the coastal Egedesminde station (Figure 7a), melt-day area in individual years normalized to 100% for the year of maximum melt (2005) (Figure 7b). The data are highly correlated (r = 0.80), suggesting 3.8% increase in melt-day area with each 0.1 K increase in temperature (Figure 7c). Temperature data are from the NASA GISS Web site (http://data.giss.nasa.gov/gistemp/station_data/).

Table 1. Relative Melt-Day Area Determined by the MADI/MODIS and AMSR-E Methods, Average Relative Temperature at Nearby Coastal Station Egedesminde, and Correlation Coefficients Between Melt-Day Area and Temperature[a]

	MADI Melt-Day Area	AMSR-E Melt-Day Area	JJA Egedesminde Temperature, T
Correlation (with T) Coefficient 2002–2006	0.91	0.47	
2000	0.82		0.90
2001	0.96		0.93
2002	0.46	0.71	0.83
2003	0.80	0.84	1.00
2004	0.56	0.99	0.87
2005	1.00	1.00	1.00
2006	0.73	0.80	0.89

[a]Average relative temperature is with respect to temperature in °C.

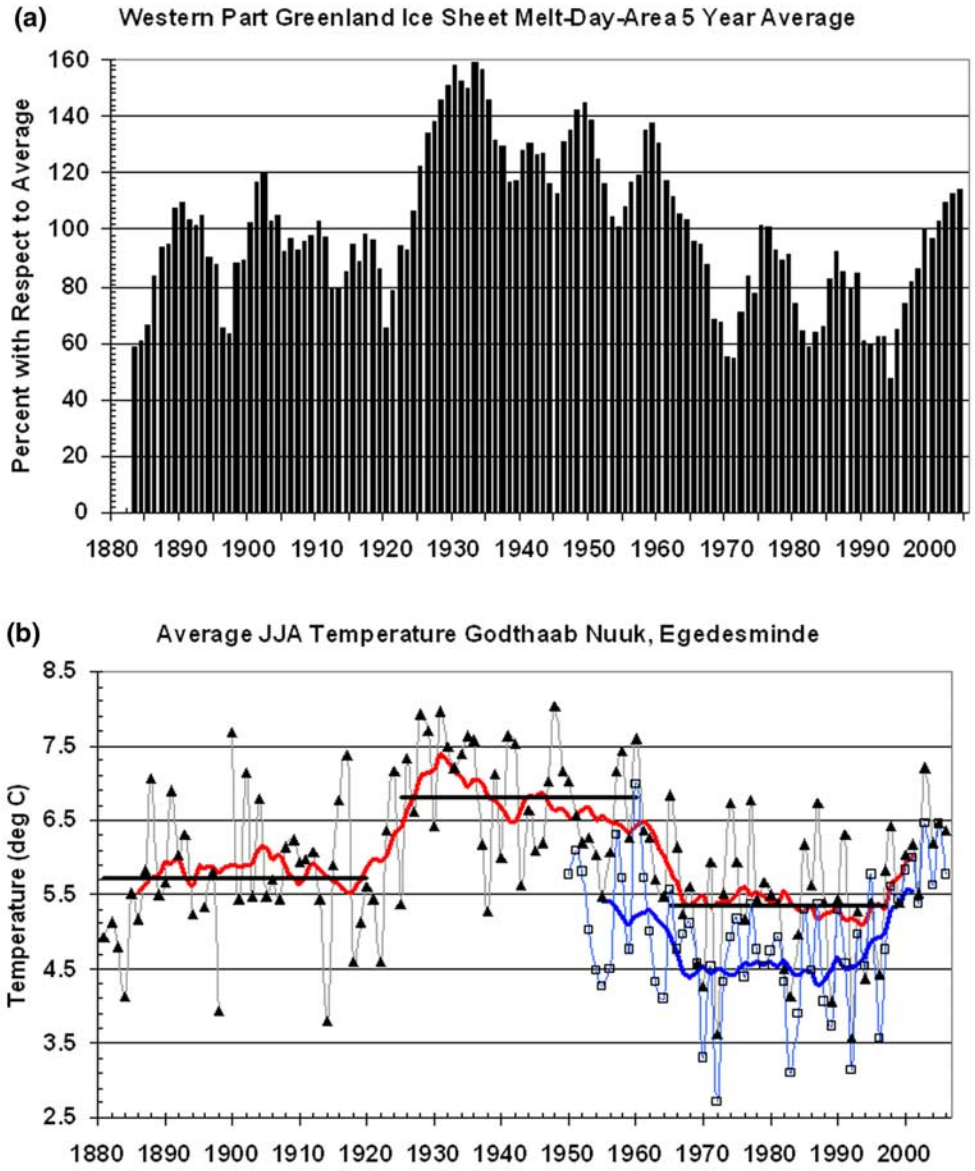

Figure 8. Figure 8a shows 5 year running average of the melt-day area of the western part of the Greenland ice sheet reconstructed from the temperature record and melt area sensitivity of 3.8% per 0.1 K temperature change. Figure 8b shows the summer (JJA) temperature at Godthaab Nuuk (solid triangles) and Egedesminde (open squares) and their 11 year running averages. Thick horizontal black lines denote average temperature within time periods of relatively stable temperature. Temperature data are from the NASA GISS Web site (http://data.giss.nasa.gov/gistemp/station_data/).

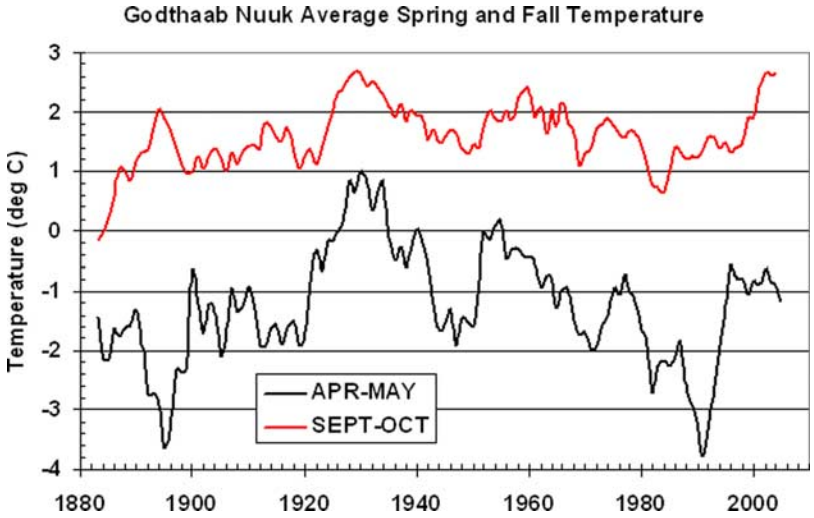

Figure 9. Five year running average of the spring (April–May) and fall (September–October) temperature at Godthaab Nuuk. Temperature data are from the NASA GISS Web site (http://data.giss.nasa.gov/gistemp/station_data/).

melt area. In our investigation of the western part of the ice sheet, we have found a high interannual variability of the melt-day area, with the maximum melt over the years 2000–2006 occurring in 2005. This was also a year of the highest summer temperature recorded in the nearby coastal station at Egedesminde. The melt-day area decreased in 2006 by over 25% compared to its 2005 value.

[26] We have found high correlation between the Egedesminde summer temperature and the melt-day area determined by the MADI/MODIS method. Our analysis suggests that it is the magnitude of the average summer temperature that dominated the melting of the western part of the ice sheet, and not the length of the melt season. An analysis of the temperature and melt-day-area data suggests that for each increase in summer average temperature of 0.1 K the melt-day area increases by about 3.8%. Extension of this relationship outside the 2000–2006 time interval suggests that the melting more than doubled between 1992 and 2005. However, the maximum amount of melting very likely occurred during the 1920s and 1930s.

[27] Our algorithm uses visible and near-infrared bands to discriminate between melting and dry snow at a high spatial resolution. It can be used to monitor the state of the Greenland ice sheet margins and outflow glaciers with a high accuracy. One obvious limitation of the optical method is that it can be used only under clear sky condition, but given the slow nature of the snow-ice melting the method should provide new insights into melting of ice sheets and glaciers. Additionally, available imagery can be merged throughout clear-sky periods to develop a composite product of the melt area dynamics. Finally, observation of seasonal and interannual changes in melting can be combined with collocated temperature measurements to develop phenomenological models and validate mechanistic models of ice sheet response to climate change. There is a pressing need for such monitoring and analysis to quantify the vulnerability of the ice sheets to anthropogenic climate change.

[28] **Acknowledgments.** The reported research (LA-UR-06-7361) was partially supported by Los Alamos National Laboratory's Directed Research and Development Project entitled "Resolving the Aerosol-Climate-Water Puzzle (20050014DR) " and by the "Mixed Phase Cloud" project supported by the University of California Institute of Geophysics and Planetary Physics.

References

Abdalati, W., and K. Steffen (1995), Passive microwave-derived snow melt regions on the Greenland ice sheet, *Geophys. Res. Lett.*, *22*, 787–790.

Abdalati, W., and K. Steffen (2001), Greenland ice sheet melt extent: 1979–1999, *J. Geophys. Res.*, *106*, 33,983–33,989.

Ahlmann, A. (1948), The present climatic fluctuation, *Geogr. J.*, *112*, 165–193.

Ashcroft, I. S., and D. G. Long (2006), Comparison of methods for melt detection over Greenland using passive and active microwave measurements, *Int. J. Remote Sens.*, *27*, 2469–2488.

Chylek, P., and C. Borel (2004), Mixed phase cloud water/ice structure from high spatial resolution satellite data, *Geophys. Res. Lett.*, *31*, L14104, doi:10.1029/2004GL020428.

Chylek, P., and U. Lohmann (2005), Ratio of the Greenland to global temperature change: Comparison of observations and climate modeling results, *Geophys. Res. Lett.*, *32*, L14705, doi:10.1029/2005GL023552.

Chylek, P., M. K. Dubey, and G. Lesins (2006a), Greenland warming of 1920–1930 and 1995–2005, *Geophys. Res. Lett.*, *33*, L11707, doi:10.1029/2006GL026510.

Chylek, P., S. Robinson, M. K. Dubey, M. D. King, Q. Fu, and W. B. Clodius (2006b), Comparison of near-infrared and thermal infrared cloud phase detections, *J. Geophys. Res.*, *111*, D20203, doi:10.1029/2006JD007140.

Colbeck, S. C. (1979), Grain clusters in wet snow, *J. Colloid Interface Sci.*, *72*, 371–384.

Dozier, J. (1989), Spectral signature of Alpine snow cover from the Landsat Thematic Mapper, *Remote Sens. Environ.*, *28*, 9–22.

Dozier, J., and T. H. Painter (2004), Multispectral and hyperspectral remote sensing of Alpine snow properties, *Annu. Rev. Earth Planet. Sci.*, *32*, 465–494.

Green, R. O., T. H. Painter, D. A. Roberts, and J. Dozier (2006), Measuring the expressed abundance of the three phases of water with an imaging spectrometer over melting snow, *Water Resour. Res.*, *42*, W10402, doi:10.1029/2005WR004509.

Hall, D. K., R. S. Williams Jr., K. A. Casey, N. E. DiGirolamo, and Z. Wan (2006), Satellite-derived, melt-season surface temperature of the Greenland Ice Sheet (2000–2005) and its relationship to mass balance, *Geophys. Res. Lett.*, *33*, L11501, doi:10.1029/2006GL026444.

Hanna, E., P. Huybrechts, I. Janssens, J. Cappelen, K. Steffen, and A. Stephens (2005), Runoff and mass balance of the Greenland ice sheet: 1958–2003, *J. Geophys. Res.*, *110*, D13108, doi:10.1029/2004JD005641.

Jackson, J. (1975), *Classical Electrodynamics*, 848 pp., John Wiley, New York.

Johannessen, O. M., K. Khvorostovsky, M. W. Miles, and L. B. Bobylev (2005), Recent ice-sheet growth in the interior of Greenland, *Science*, *310*, 1013–1016.

King, M. D., Y. J. Kaufman, W. P. Menzel, and D. Tanré (1992), Remote sensing of cloud, aerosol, and water vapor properties from the Moderate Resolution Imaging Spectrometer (MODIS), *IEEE Trans. Geosci. Remote Sens.*, *30*, 2–27.

King, M. D., S. Platnick, P. Yang, G. T. Arnold, M. A. Gray, J. C. Riédi, S. A. Ackerman, and K. N. Liou (2004), Remote sensing of liquid water and ice cloud optical thickness and effective radius in the Arctic: Application of airborne multispectral MAS data, *J. Atmos. Ocean Technol.*, *21*, 857–875.

Kou, L., D. Labrie, and P. Chylek (1993), Refractive index of water and ice in the 0.65 to 2.5 μm spectral range, *Appl. Opt.*, *32*, 3531–3540.

Luthcke, S. B., H. J. Zwally, W. Abdalati, D. D. Rowlands, R. D. Ray, R. S. Nerem, F. G. Lemoine, J. J. McCarthy, and D. S. Chinn (2006), Recent Greenland ice mass loss by drainage system from satellite gravity observations, *Science*, *314*, 1286–1289.

Remer, L. A., et al. (2005), The MODIS aerosol algorithm, products, and validation, *J. Atmos. Sci.*, *62*, 947–973.

Steffen, K., S. V. Nghiem, R. Huff, and G. Neumann (2004), The melt anomaly of 2002 on the Greenland Ice Sheet from active and passive microwave satellite observations, *Geophys. Res. Lett.*, *31*, L20402, doi:10.1029/2004GL020444.

Stroeve, J., and K. Steffen (1998), Variability of AVHRR-derived clear-sky surface temperature over the Greenland ice sheet, *J. Appl. Meteorol.*, *37*, 23–31.

Stroeve, J. C., J. Box, F. Gao, S. Liang, A. Nolin, and C. Schaaf (2005), Accuracy assessment of the MODIS 16–albedo product for snow: Comparison with Greenland in situ measurements, *Remote Sens. Environ.*, *94*, 46–60.

Szymanski, J., and P. Weber (2005), Multispectral Thermal Imager: Mission and applications overview, *IEEE Trans. Geosci. Remote Sens.*, *43*, 1943–1949.

Tanré, D., Y. Kaufman, M. Herman, and S. Mattoo (1997), Remote sensing of aerosol properties over oceans using the MODIS/EOS spectral radiances, *J. Geophys. Res.*, *102*, 16,971–16,988.

Vinther, B. M., K. K. Andersen, P. D. Jones, K. R. Briffa, and J. Cappelen (2006), Extending Greenland temperature records into the late eighteenth century, *J. Geophys. Res.*, *111*, D11105, doi:10.1029/2005JD006810.

Zwally, J., et al. (2005), Mass changes of the Greenland and Antarctic ice sheets and shelves and contributions to sea-level rise: 1992–2002, *J. Glaciol.*, *51*, 509–527.

P. Chylek and M. McCabe, Space and Remote Sensing, Los Alamos National Laboratory, Los Alamos, NM 87545, USA. (chylek@lanl.gov)

J. Dozier, Donald Bren School of Environmental Science and Management, University of California, Santa Barbara, Santa Barbara, CA 93106-5131, USA.

M. K. Dubey, Earth and Environmental Sciences, Los Alamos National Laboratory, Los Alamos, NM 87545, USA.